ZZ production at the LHC: NNLO predictions for $2\ell2\nu$ and 4ℓ signatures

Stefan Kallweit [*], Marius Wiesemann [*]

TH Division, Physics Department, CERN, CH-1211 Geneva 23, Switzerland

ABSTRACT

We consider QCD radiative corrections to ZZ production for all experimentally relevant leptonic processes. We report on a novel computation of next-to-next-to-leading-order (NNLO) corrections to the diboson signature with two charged leptons and missing transverse energy ($\ell\ell + E_T^{\text{miss}}$). All relevant final states are considered: $\ell\ell\nu_\ell\nu_\ell$, $\ell\ell\nu_{\ell'}\nu_{\ell'}$ and $\ell\nu_\ell\ell'\nu_{\ell'}$. We also study processes with four charged leptons: $\ell\ell\ell\ell$ and $\ell\ell\ell'\ell'$. For the first time NNLO accuracy is achieved for a process mixing two double-resonant diboson topologies ($ZZ/W^+W^- \to \ell\ell\nu_\ell\nu_\ell$). We find good agreement with ATLAS data at 8 TeV. NNLO corrections are large (5–20% and more), and interference effects between ZZ and W^+W^- resonances turn out to be negligible in most cases.

© 2018 The Authors. Published by Elsevier B.V. This is an open access article under the CC BY license (http://creativecommons.org/licenses/by/4.0/). Funded by SCOAP³.

Diboson processes play a major role in the rich physics programme of the LHC. The intriguing nature of these processes combined with their rather clean experimental signatures and relatively large cross sections render them ideal for Standard Model (SM) precision measurements. The precise knowledge of diboson rates and distributions provides a strong test of the gauge-symmetry structure of electroweak (EW) interactions and the mechanism of EW symmetry breaking. They also serve as important probes of new physics phenomena in direct and indirect searches. Diboson final states, in particular ZZ and W^+W^-, are also extensively used in Higgs-boson measurements.

The production of ZZ pairs yields the smallest cross section among the diboson processes. Nevertheless, its pure experimental signature with four charged leptons in the final state facilitates a clean measurement so that it has already been used in a combination of ATLAS and CMS data to constrain anomalous trilinear gauge couplings [1]. ZZ production at the LHC has been measured at 7 TeV [2–4], 8 TeV [5–9], and 13 TeV [10–13]. Also searches for new heavy ZZ resonances involving both charged leptons and neutrinos have been performed, see Ref. [14] for example.

Theoretical predictions for ZZ production at next-to-leading order (NLO) QCD were obtained a long time ago for both on-shell Z bosons [15,16] and their fully leptonic final states [17–20]. Perturbative corrections beyond NLO QCD are indispensable to reach the precision demanded by present ZZ measurements. NLO EW corrections are known for stable Z bosons [21–23] and including their full off-shell treatment for leptonic final states [24–26]. $ZZ + $ jet production was computed at NLO QCD [27]. The loop-induced $gg \to ZZ + X$ subprocess, which provides a separately finite $\mathcal{O}(\alpha_S^2)$ contribution, is known at leading order (LO) [28–38] and was recently computed at NLO considering only gg-initiated partonic channels [39–41], using the two-loop helicity amplitudes for $gg \to VV'$ of Refs. [42,43]. NNLO QCD corrections to on-shell ZZ production were first evaluated in Ref. [44], and later in Ref. [45]. Using the two-loop helicity amplitudes for $q\bar{q} \to VV'$ [46–48], differential predictions in the four-lepton channels ($\ell\ell\ell\ell$ and $\ell\ell\ell'\ell'$) were presented in Ref. [49].

In this paper we complete NNLO QCD corrections to ZZ production by considering all experimentally relevant leptonic final states. Our computations are fully differential in the momenta of the final-state leptons, and we account for off-shell effects and spin correlations by consistently including all resonant and non-resonant topologies. For the first time, we obtain NNLO-accurate predictions for the (same-flavour) dilepton plus missing transverse energy signature ($\ell\ell + E_T^{\text{miss}}$), which involves all processes with two opposite-charge leptons and two neutrinos in the final state ($\ell\ell\nu_\ell\nu_\ell$, $\ell\ell\nu_{\ell'}\nu_{\ell'}$ and $\ell\nu_\ell\ell'\nu_{\ell'}$). The process $\ell\ell\nu_\ell\nu_\ell$ is particularly interesting as it mixes ZZ and W^+W^- topologies, which will be studied in detail. For completeness we also compute NNLO corrections to the four-lepton channels ($\ell\ell\ell\ell$ and $\ell\ell\ell'\ell'$). Phenomenological predictions at NNLO for all of the aforementioned leptonic processes are compared to LHC data at 8 TeV.

* Corresponding authors.
E-mail addresses: stefan.kallweit@cern.ch (S. Kallweit), marius.wiesemann@cern.ch (M. Wiesemann).
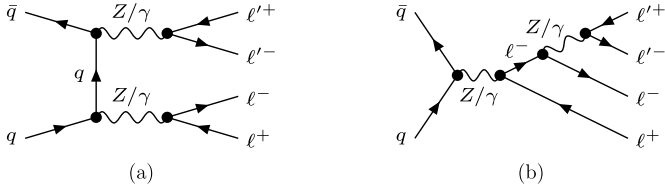
Fig. 1. Born-level Feynman diagrams for ZZ production with four charged final-state leptons.

We employ the computational framework MATRIX [50]. All tree-level and one-loop amplitudes are evaluated with OPENLOOPS[1] [55, 56]. At two-loop level we use the $q\bar{q} \to VV'$ amplitudes of Ref. [48], and implement the leptonic final states with two charged leptons and two neutrinos as well as with four charged leptons. NNLO accuracy is achieved by a fully general implementation of the q_T-subtraction formalism [57] within MATRIX. The NLO parts therein (for ZZ and $ZZ + 1$-jet) are performed by MUNICH[2] [60], which employs the Catani–Seymour dipole subtraction method [61, 62]. The MATRIX framework features NNLO QCD corrections to a large number of colour-singlet processes at hadron colliders, and has already been used to obtain several state-of-the-art NNLO predictions [44,49,63–70].[3]

We consider all leptonic signatures relevant for ZZ measurements at the LHC. On the one hand, we compute the four-lepton (4ℓ) processes

$$pp \to \ell^+\ell^-\,\ell'^+\ell'^- + X,$$

with different-flavour (DF) leptons ($\ell \neq \ell'$), denoted as $\ell\ell\ell'\ell'$, and same-flavour (SF) leptons ($\ell = \ell'$), denoted as $\ell\ell\ell\ell$. Representative LO diagrams are shown in Fig. 1. They involve both double-resonant t-channel ZZ production (panel a) and single-resonant s-channel Drell–Yan (DY) topologies (panel b). On the other hand, we compute processes with two charged leptons and two neutrinos ($2\ell2\nu$) in the final state,

$$pp \to \ell^+\ell^-\,\nu_{\ell'}\bar{\nu}_{\ell'} + X, \quad pp \to \ell^+\nu_\ell\,\ell'^-\bar{\nu}_{\ell'} + X,$$

$$\text{and } pp \to \ell^+\ell^-\,\nu_\ell\bar{\nu}_\ell + X, \quad \text{with } \ell \neq \ell'.$$

Representative LO diagrams are shown in Fig. 2. In the first process the flavour of the neutrinos does not match the flavour of the charged leptons, and it features double-resonant ZZ contributions (panel a) as well as DY-type topologies (panel b). In the second process the two charged leptons are of different flavours, and it features double-resonant W^+W^- contributions (panels c and d) as well as DY-type topologies (panel e). In the third process all leptons and neutrinos are of the same flavour, and the topologies of the first two processes mix in the matrix elements.

All of the aforementioned processes with charged leptons $\ell, \ell' \in \{e, \mu\}$ and neutrinos $\nu_\ell, \nu_{\ell'} \in \{\nu_e, \nu_\mu, \nu_\tau\}$ are studied. The loop-induced gg component is part of the NNLO corrections to these processes and therefore included. The same is true for resonant Higgs-boson topologies, which also start contributing at $\mathcal{O}(\alpha_s^2)$.

A significant complication of the processes $pp \to \ell^+\nu_\ell\,\ell'^-\bar{\nu}_{\ell'}$ and $pp \to \ell^+\ell^-\,\nu_\ell\bar{\nu}_\ell$ is posed by the contamination from resonant top-quark contributions with $t \to Wb$ decays, which enters

radiative corrections through diagrams featuring external bottom quarks. In the context of W^+W^- production [65,66] two approaches were followed: A top-free W^+W^- cross section can be obtained in the four-flavour scheme (4FS) by dropping all contributions with real bottom quarks, which are separately finite due to the bottom-quark mass. Since in the five-flavour scheme (5FS) real and virtual contributions of massless bottom quarks are inevitably tied together, the resonance structure of top-quark contributions is exploited to determine a top-free cross section. Neither of the two approaches is required in the case of the ZZ measurements presented here. Since W^+W^- and top-quark processes are both treated as backgrounds in the respective experimental analyses, we introduce the following procedure: First, we compute the SF process $pp \to \ell^+\ell^-\,\nu_\ell\bar{\nu}_\ell$ including all resonant contributions. In order to keep only ZZ topologies (and interferences), we then subtract the DF process $pp \to \ell^+\nu_\ell\,\ell'^-\bar{\nu}_{\ell'}$. This removes W^+W^- and top-quark backgrounds from our predictions, as desired, while their interference with ZZ production, which is not accounted for in the background predictions and thus considered part of the ZZ signal, is kept. Its impact will be studied in detail below. If W^+W^- or top-quark topologies yield much larger contributions than ZZ to the SF process, sizeable cancellations in the subtraction could diminish the numerical accuracy of our predictions. However, for typical ZZ signal cuts, as considered here, a Z-mass window suppresses the W^+W^- contribution, and a jet veto the top-quark background. The presented procedure applies in all flavour schemes, and we conveniently use the 5FS throughout.

We present predictions for the 8 TeV LHC. For the EW parameters we employ the G_μ scheme and compute the EW mixing angle as $\cos\theta_W^2 = (m_W^2 - i\Gamma_W m_W)/(m_Z^2 - i\Gamma_Z m_Z)$ and $\alpha = \sqrt{2}\,G_\mu m_W^2 \sin^2\theta_W/\pi$, using the complex-mass scheme [73] throughout. The EW inputs are set to the PDG [74] values: $G_F = 1.16639 \times 10^{-5}$ GeV^{-2}, $m_W = 80.385$ GeV, $\Gamma_W = 2.0854$ GeV, $m_Z = 91.1876$ GeV, $\Gamma_Z = 2.4952$ GeV, $m_H = 125$ GeV, and $\Gamma_H = 0.00407$. The branching ratio of the Z-boson decay into massless charged leptons, $\ell \in \{e, \mu\}$, is BR$(Z \to \ell\ell) = 0.033631$, which is used below to compute the cross section in the total phase space. The on-shell top-quark mass is set to $m_t = 173.2$ GeV, and $\Gamma_t = 1.44262$ is used. For each perturbative order we use the corresponding set of $N_f = 5$ NNPDF3.0 [75] parton distributions with $\alpha_S(m_Z) = 0.118$. Renormalization (μ_R) and factorization (μ_F) scales are set to half of the invariant mass of the ZZ pair, $\mu_R = \mu_F = \mu_0 \equiv \frac{1}{2}m_{ZZ}$. Residual uncertainties are estimated from customary 7-point scale variations by a factor of two, with the constraint $0.5 \leq \mu_R/\mu_F \leq 2$.

We start by comparing phenomenological predictions to the ATLAS 8 TeV measurement of Ref. [9]. The corresponding phase-space cuts are summarized in Table 1 for both the four-lepton and the $\ell\ell + E_T^{\text{miss}}$ signatures. The total phase space is defined by a Z-mass window in the invariant mass of each reconstructed Z boson. The reconstruction is unambiguous in the DF channel $\ell\ell\ell'\ell'$, $Z_a^{\text{rec}} = \ell^+\ell^-$ and $Z_b^{\text{rec}} = \ell'^+\ell'^-$, which we employ for the predicted cross sections in the total phase space. The fiducial cuts involve standard requirements on the transverse momenta and pseudo-rapidities of the leptons, a separation in $\Delta R = \sqrt{\Delta\eta^2 + \Delta\phi^2}$ between the leptons, and a window in the invariant mass of reconstructed Z bosons around the Z-pole. In the SF channel $\ell\ell\ell\ell$, Z bosons are reconstructed by identifying the combination of opposite-sign same-flavour (OSSF) lepton pairings ($Z_a = \ell_a^+\ell_a^-$ and $Z_b = \ell_b^+\ell_b^-$, or $Z_a = \ell_a^+\ell_b^-$ and $Z_b = \ell_b^+\ell_a^-$) that minimizes $\left|m_{Z_a} - m_Z\right| + \left|m_{Z_b} - m_Z\right|$ with the reconstructed Z bosons $Z_a^{\text{rec}} = Z_a$ and $Z_b^{\text{rec}} = Z_b$. A rather special feature in the fiducial phase spaces of the four-lepton channels is the fact that ATLAS measures one of the electrons up to very large pseudo-rapidities ($|\eta_e| < 4.9$). The measurement of the $\ell\ell + E_T^{\text{miss}}$ signature applies two additional requirements, which

---

[1] OPENLOOPS relies on the fast and stable tensor reduction of COLLIER [51,52], supported by a rescue system based on quad-precision CUTTOOLS [53] with ONELOOP [54] to deal with exceptional phase-space points.

[2] The Monte Carlo program MUNICH features a general implementation of an efficient, multi-channel based phase-space integration and computes both NLO QCD and NLO EW [58,59] corrections to arbitrary SM processes.

[3] It was also used in the NNLL+NNLO computation of Ref. [71], and in the NNLOPS computation of Ref. [72].
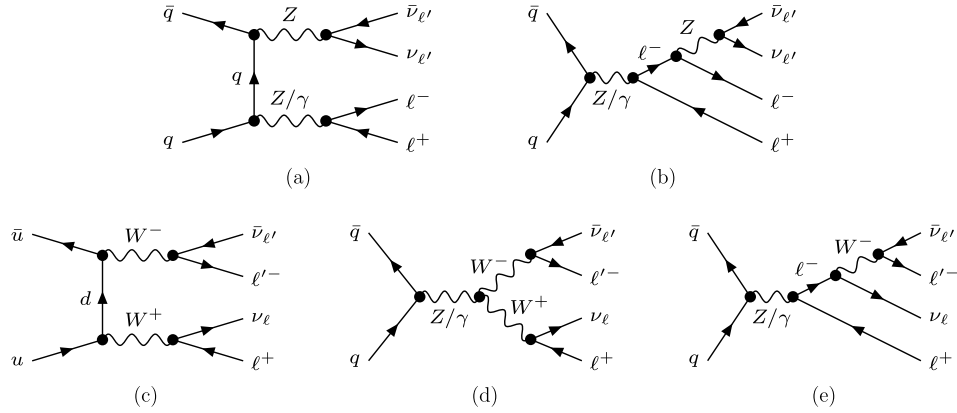
Fig. 2. Born-level Feynman diagrams for the production of two charged leptons and two neutrinos: (a–b) topologies of ZZ production contributing to the process $pp \rightarrow \ell^+\ell^-\nu_{\ell'}\bar{\nu}_{\ell'}$ ($\ell \neq \ell'$); (c–e) topologies of W^+W^- production contributing to the process $pp \rightarrow \ell^+\nu_\ell\ell'^-\bar{\nu}_{\ell'}$ ($\ell \neq \ell'$); for $\ell = \ell'$ all diagrams contribute to the process $pp \rightarrow \ell^+\ell^-\nu_\ell\bar{\nu}_\ell$, thereby mixing ZZ and W^+W^- topologies.

Table 1
Phase-space definitions of the ZZ measurements by ATLAS at 8 TeV [9].

definition of the total phase space for $pp \rightarrow ZZ + X$
66 GeV $\leq m_{Z^{rec}_{a/b}} \leq$ 116 GeV
definition of the fiducial volume for $pp \rightarrow \ell^+\ell^-\ell'^+\ell'^- + X$, $\ell, \ell' \in \{e, \mu\}$
$p_{T,\ell} > 7$ GeV, one electron with $|\eta_e| < 4.9$, the others $|\eta_e| < 2.5$, $|\eta_\mu| < 2.7$ $\Delta R_{\ell\ell} > 0.2$, $\Delta R_{\ell\ell'} > 0.2$, 66 GeV $\leq m_{Z^{rec}_{a/b}} \leq$ 116 GeV, anti-k_T jets with $R = 0.4$, $p_{T,j} > 25$ GeV, $|\eta_j| < 4.5$ lepton identification in SF channel: minimizing differences of invariant-mass of OSSF lepton pairs and m_Z
definition of the fiducial volume for $pp \rightarrow \ell^+\ell^-\nu\bar{\nu} + X$, $\ell \in \{e, \mu\}$ and $\nu \in \{\nu_e, \nu_\mu, \nu_\tau\}$
$p_{T,\ell} > 25$ GeV, $|\eta_\ell| < 2.5$, $\Delta R_{\ell\ell} > 0.3$, 76 GeV $\leq m_{\ell^+\ell^-} \leq$ 106 GeV, Axial-$p_T^{miss} > 90$ GeV, p_T-balance < 0.4, $N_{jets} = 0$, anti-k_T jets with $R = 0.4$, $p_{T,j} > 25$ GeV, $|\eta_j| < 4.5$ and $\Delta R_{ej} > 0.3$

force the two Z bosons closer to back-to-back-like configurations to suppress backgrounds such as Z + jets: There is a lower cut on the axial missing transverse momentum, Axial-$p_T^{miss} = -p_T^{miss} \cdot \cos(\Delta\phi_{\ell\ell,\nu\nu})$, where $p_T^{miss} \equiv p_{T,\nu\nu}$ and $\Delta\phi_{\ell\ell,\nu\nu}$ is the azimuthal angle between the dilepton and the neutrino pair. Furthermore, the two Z-boson momenta are balanced by putting an upper cut on p_T-balance $= |p_T^{miss} - p_{T,\ell\ell}|/p_{T,\ell\ell}$. Finally, the $\ell\ell + E_T^{miss}$ signature requires a jet veto to suppress top-quark backgrounds. Note that jets close to electrons ($\Delta R_{ej} < 0.3$) are not vetoed.

In Table 2 we report cross-section predictions and compare them against ATLAS 8 TeV results [9]. Central predictions are stated with the numerical error on the last digit quoted in round brackets. The relative uncertainties quoted in percent are estimated from scale variations as described above. Results reported for $e^+e^-\mu^+\mu^-$, $e^+e^-e^+e^-$, $\mu^+\mu^-\mu^+\mu^-$, $e^+e^-\nu\bar{\nu}$, and $\mu^+\mu^-\nu\bar{\nu}$ production are cross sections in the respective fiducial volumes defined in Table 1. The prediction in the last line of the table is obtained from the computation of $pp \rightarrow e^+e^-\mu^+\mu^- + X$ in the

total phase space defined in Table 1, by dividing out the branching ratio BR($Z \rightarrow \ell\ell$) for each Z-boson decay. The main conclusions that can be drawn from these results are the following:

- Radiative corrections are large and have a marked dependence on the event selection: They range between +35% to +40% at NLO and +14% to +17% at NNLO in cases without a jet veto, i.e. for all but the $2\ell 2\nu$ results. Roughly half (45%–55%) of the $\mathcal{O}(\alpha_s^2)$ terms are due to the loop-induced gg component in these cases. For the $2\ell 2\nu$ processes the situation is quite different: Due to the jet veto NLO corrections turn negative and yield about -14%. NNLO corrections are roughly +6%. However, the positive effect is entirely due to loop-induced gg contributions, which are not affected by the jet veto. Omitting the loop-induced gg terms, the genuine NNLO corrections to the $q\bar{q}$ channel are actually negative and about -5%. Hence, despite the jet veto, full $\mathcal{O}(\alpha_s^2)$ corrections are crucial for the $\ell\ell + E_T^{miss}$ signature.

- For channels with four charged leptons we find good agreement between theory and data. This is particularly true for the DF process ($e^+e^-\mu^+\mu^-$), where NNLO corrections clearly improve the comparison. In the SF channels ($e^+e^-e^+e^-$ and $\mu^+\mu^-\mu^+\mu^-$) NNLO predictions are slightly larger than the measurements, but remain within 1σ for muons and 2σ for electrons. One should not forget that EW corrections reduce the rates by a few percent [25], while NLO corrections to the loop-induced gg channel have a positive effect [39].

- For the $\ell\ell + E_T^{miss}$ signatures excellent agreement is found between NNLO predictions and measured cross sections. It is worth noting that fixed-order results describe the data significantly better than the POWHEG [76–79] Monte Carlo prediction used in Ref. [9]. This could be caused by the jet-veto requirement: As pointed out in Ref. [80] for W^+W^- production, in

Table 2
Predictions for fiducial and total rates compared to ATLAS 8 TeV data [9].

| Channel	σ_{LO} [fb]	σ_{NLO} [fb]	σ_{NNLO} [fb]	σ_{ATLAS} [fb]
$e^+e^-\mu^+\mu^-$	8.188(1)$^{+2.4\%}_{-3.2\%}$	11.30(0)$^{+2.5\%}_{-2.0\%}$	12.92(1)$^{+2.8\%}_{-2.2\%}$	12.4$^{+1.0}_{-1.0}$(stat)$^{+0.6}_{-0.5}$(syst)$^{+0.3}_{-0.2}$(lumi)
$e^+e^-e^+e^-$	4.654(0)$^{+2.3\%}_{-3.1\%}$	6.410(2)$^{+2.5\%}_{-2.0\%}$	7.310(8)$^{+2.7\%}_{-2.1\%}$	5.9$^{+0.8}_{-0.8}$(stat)$^{+0.4}_{-0.4}$(syst) $\pm$ 0.1(lumi)
$\mu^+\mu^-\mu^+\mu^-$	3.565(0)$^{+2.6\%}_{-3.5\%}$	4.969(5)$^{+2.5\%}_{-2.0\%}$	5.688(6)$^{+2.9\%}_{-2.2\%}$	4.9$^{+0.6}_{-0.5}$(stat)$^{+0.3}_{-0.2}$(syst) $\pm$ 0.1(lumi)
$e^+e^-\nu\nu$	5.558(0)$^{+0.1\%}_{-0.5\%}$	4.806(1)$^{+3.5\%}_{-3.9\%}$	5.083(8)$^{+1.9\%}_{-0.6\%}$	5.0$^{+0.8}_{-0.7}$(stat)$^{+0.5}_{-0.4}$(syst) $\pm$ 0.1(lumi)
$\mu^+\mu^-\nu\nu$	5.558(0)$^{+0.1\%}_{-0.5\%}$	4.770(4)$^{+3.6\%}_{-4.0\%}$	5.035(9)$^{+1.8\%}_{-0.5\%}$	4.7$^{+0.7}_{-0.7}$(stat)$^{+0.5}_{-0.4}$(syst) $\pm$ 0.1(lumi)
total rate	4982(0)$^{+1.9\%}_{-2.7\%}$	6754(2)$^{+2.4\%}_{-2.0\%}$	7690(5)$^{+2.7\%}_{-2.1\%}$	7300$^{+400}_{-400}$(stat)$^{+300}_{-300}$(syst)$^{+200}_{-100}$(lumi)
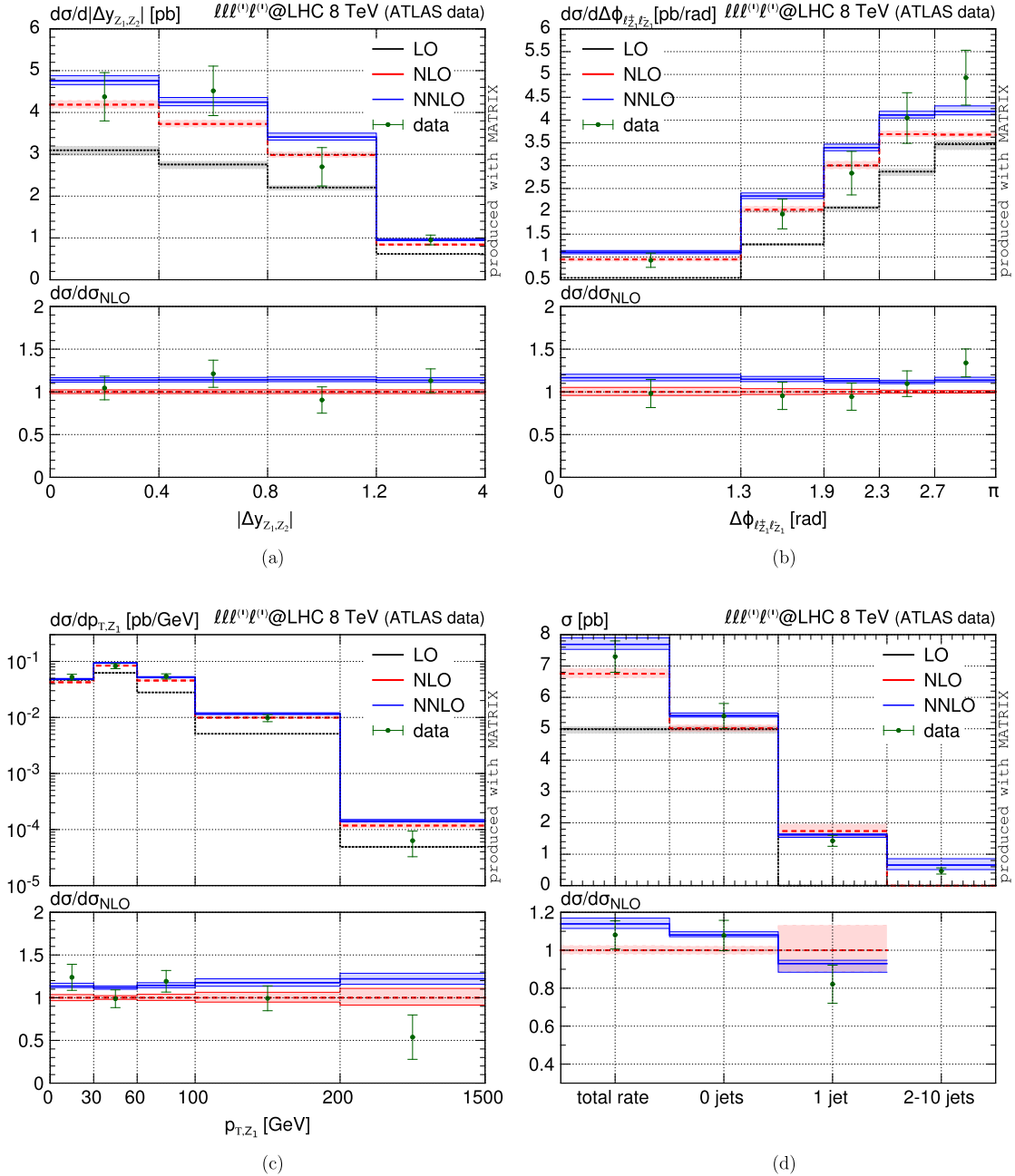
Fig. 3. Differential distributions for the four-lepton processes in the total phase space at LO (black, dotted), NLO (red, dashed) and NNLO (blue, solid), compared to ATLAS 8 TeV data extrapolated to the total phase space [9] (green points with error bars); for (a) $\Delta y_{Z_1,Z_2}$, (b) $\Delta\phi_{\ell^+_{Z_1},\ell^-_{Z_1}}$, (c) p_{T,Z_1}, and (d) N_{jets}; the lower frames show the ratio over NLO.

presence of a jet veto the fiducial rate predicted by POWHEG is rather small.

- The NNLO prediction in the last line of the table agrees perfectly ($< 1\sigma$) with the experimental result in the total phase space, with NNLO corrections being crucial for this level of agreement.

- At LO scale uncertainties clearly underestimate the actual size of higher-order corrections, since only the $q\bar{q}$ channel contributes and the cross section is μ_R-independent. Given large NLO corrections, also the scale uncertainties of 2%–4% at NLO cannot be trusted as an estimate of missing higher-order terms. However, at NNLO all partonic channels are included, and the corrections to the $q\bar{q}$ channel, which are much smaller than at NLO, are of the same order as the respective scale

variations. Therefore, NNLO uncertainties may be expected to reflect the size of yet un-calculated perturbative corrections to this channel. Only the loop-induced gg component underestimates the uncertainty due to its LO nature, which is known from the sizable NLO contributions to the gg channel [39].

We now turn to discussing differential distributions. Fig. 3 shows results for the production of four charged leptons in the total phase space. Theoretical predictions in these plots are obtained from the DF process $pp \to e^+e^- \mu^+\mu^- + X$, divided by the branching ratio BR($Z \to \ell\ell$) for each Z-boson decay. The measured results are extrapolated to the total phase space, as presented by ATLAS at 8 TeV [9]. Given that one electron is measured up to absolute pseudo-rapidities of 4.9, the extrapolation factor, and pos-
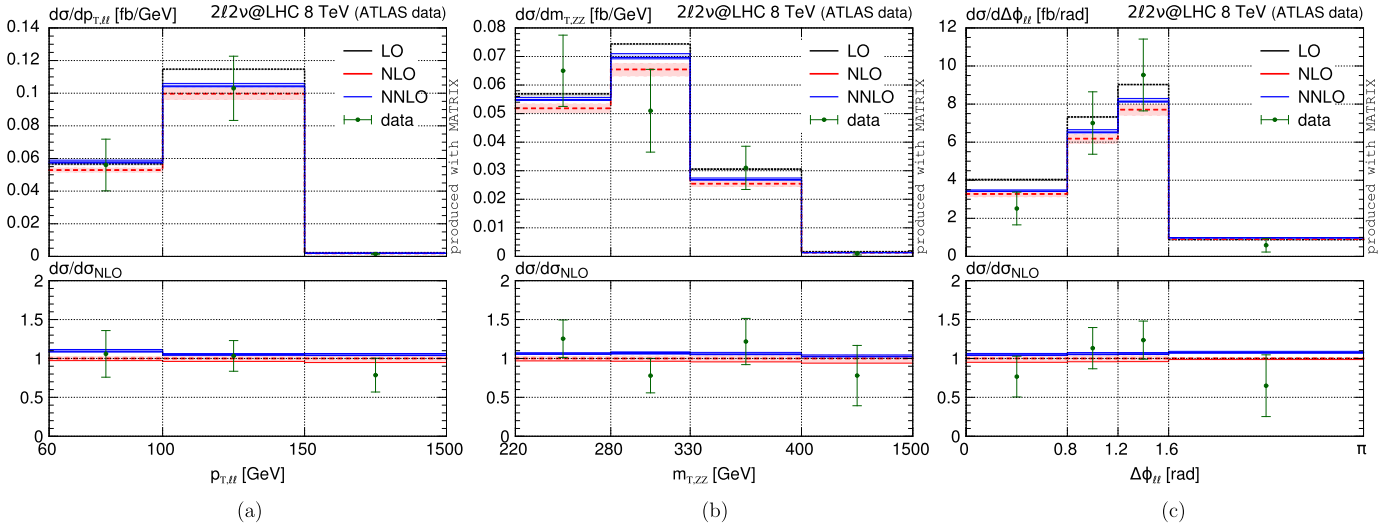
Fig. 4. Differential distributions of the $2\ell 2\nu$ processes with fiducial cuts at LO (black, dotted), NLO (red, dashed) and NNLO (blue, solid), compared to ATLAS 8 TeV data [9] (green points with error bars); for (a) $p_{T,\ell\ell}$, (b) $m_{T,ZZ}$, and (c) $\Delta\phi_{\ell\ell}$; the lower frame shows the ratio over NLO.

sibly the ensuing uncertainty, is smaller than in other four-lepton measurements. Nevertheless, we reckon that a direct comparison against unfolded distributions in the fiducial volume is preferable, as it is less affected by the lower perturbative accuracy of the Monte Carlo generator used for the extrapolation. However, since no such experimental results are available in the four-lepton channel from ATLAS at 8 TeV, we perform the comparison in the total phase space. We have normalized the ATLAS distributions to the measured total cross section in the last line of Table 2.

Despite the fact that the comparison is done in the total phase space, theory predictions and measured cross sections are in reasonable agreement for the observables shown in Fig. 3, which are the rapidity difference of the reconstructed Z bosons, $\Delta y_{Z_1,Z_2}$ (panel a), the azimuthal angle between the two leptons of the harder Z boson, $\Delta\phi_{\ell_{Z_1}^+,\ell_{Z_1}^-}$ (panel b), the transverse momentum of the leading Z boson, p_{T,Z_1} (panel c), and the number of jets, N_{jets} (panel d). Overall, NNLO predictions provide the best description of data, although NLO results are similarly close, while LO is far off. Note that for the jet multiplicity the effective perturbative accuracy of the (fixed-order) predictions is degraded by one order for each added jet. NNLO effects on other distributions are large, but primarily affect the normalization and not the shapes.

We continue our discussion of differential results with the $\ell\ell + E_T^{\text{miss}}$ signature in Fig. 4, which shows the distributions in the transverse momentum of the dilepton pair, $p_{T,\ell\ell}$ (panel a), the transverse mass of the ZZ pair, defined as[4]

$$m_{T,ZZ}$$
$$= \sqrt{\left(\sqrt{p_{T,\ell\ell}^2 + m_Z^2} + \sqrt{(p_T^{\text{miss}})^2 + m_Z^2}\right)^2 - (\mathbf{p}_{T,\ell\ell} + \mathbf{p}_T^{\text{miss}})^2}$$

(panel b), and the azimuthal angle between the two leptons, $\Delta\phi_{\ell\ell}$ (panel c). The results correspond to the sum of all channels including both SF ($\ell\ell\,\nu_\ell\nu_\ell$) and DF ($\ell\ell\,\nu_{\ell'}\nu_{\ell'}$) processes ($\ell \in \{e,\mu\}$, $\nu_{\ell'} \in \{\nu_e,\nu_\mu,\nu_\tau\}$, $\ell \neq \ell'$). We recall that SF contributions are computed by subtracting W^+W^- and top-quark backgrounds as outlined before. For all three distributions in Fig. 4 we find excellent agreement between theory and data. At NNLO, differences

hardly exceed the 1σ level. Although NNLO corrections change the cross section in certain bins, the experimental uncertainties are still too large for more distinct conclusions. Similar to our previous observations for fiducial rates, the agreement found here at fixed order is a significant improvement over the comparison with the Monte Carlo prediction shown in Ref. [9]. As pointed out before, we expect a poor modelling of the jet veto by the POWHEG generator to be the main source of these differences, see also Ref. [80].

In the remainder of this paper we focus on the $\ell\ell + E_T^{\text{miss}}$ signature, with the same fiducial setup as before. In Fig. 5 we have picked three out of many observables where the importance of NNLO corrections is evident. The NLO$'$ + gg result in the ratio frame denotes the sum of the NLO and the loop-induced gg cross section, both evaluated with NNLO PDFs, which was the best prediction available in the past. Its difference compared to the complete NNLO QCD result shows the size of the genuine $\mathcal{O}(\alpha_S^2)$ corrections to the $q\bar{q}$ channel, computed for the first time in this paper. For example, the $\Delta\phi_{\ell\ell}$ distribution in Fig. 5 (panel a) develops a sizable NNLO/NLO K-factor up to 1.6 for large separations. From the considerable differences between NNLO and NLO$'$ + gg curves, which also concern their shapes, it is clear that this effect stems directly from the newly computed $\mathcal{O}(\alpha_S^2)$ contributions. In this phase-space region (large $\Delta\phi_{\ell\ell}$) the perturbative accuracy is effectively diminished by one order due to the phase-space cuts which force the two Z bosons to be boosted and approximately back-to-back, so that the two decay leptons disfavour large separations. This manifests itself also in a widening of the scale uncertainty bands. Also the transverse-momentum spectrum of the hardest lepton, p_{T,ℓ_1} in Fig. 5 (panel b) features a significant shape distortion at NNLO, when compared to both NLO and NLO$'$ + gg. The same is true for the missing transverse momentum, p_T^{miss} in Fig. 5 (panel c). In all cases perturbative uncertainties are clearly reduced upon inclusion of higher-order corrections.

We complete our discussion of phenomenological results by studying the size of ZZ, W^+W^-, and interference contributions entering the SF process $pp \to \ell^+\ell^-\,\nu_\ell\bar{\nu}_\ell$. We recall that W^+W^- contributions also involve resonant top-quark topologies. In contrast to our previous discussion, W^+W^- and top-quark contributions are not subtracted from the SF process in the following. We focus on the contamination of the $\ell\ell + E_T^{\text{miss}}$ signature through interference with W^+W^- and top-quark diagrams. To this end, Fig. 6 compares the NNLO cross section for the full process of two OSSF leptons and two neutrinos, $\sigma(\ell\ell\,\nu_{e/\mu/\tau}\nu_{e/\mu/\tau}) =$
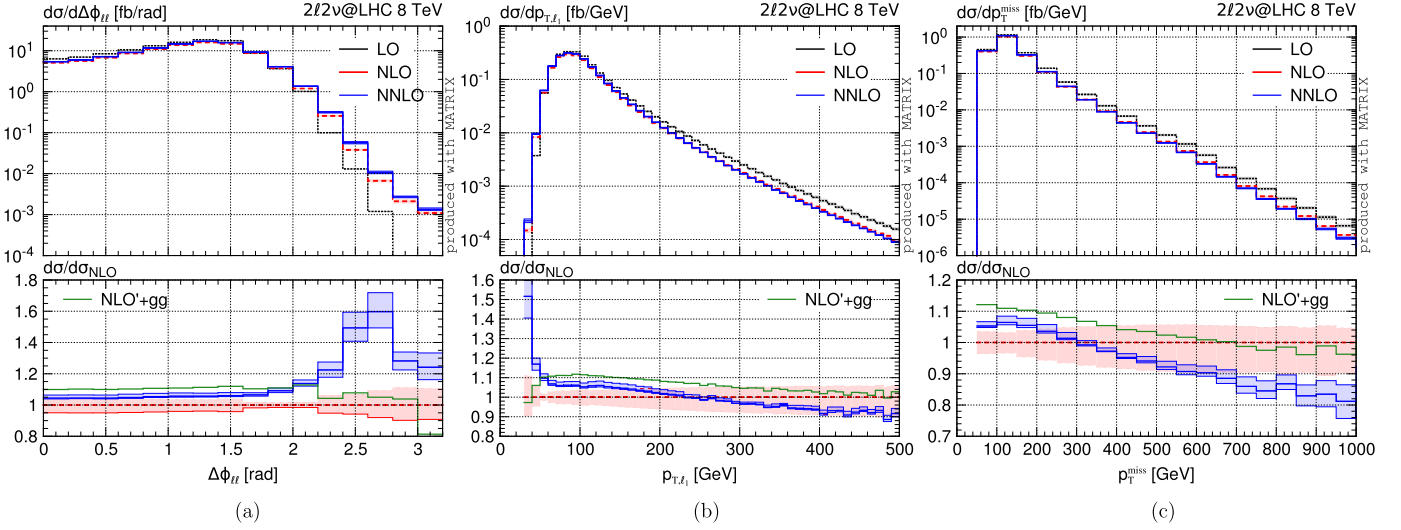
---

[4] Boldface is used to indicate the vectorial sum of the dilepton and missing transverse momentum.

Fig. 5. Same as Fig. 4, but without data and for the distributions (a) $\Delta\phi_{\ell\ell}$, (b) p_{T,ℓ_1}, and (c) p_T^{miss}; for reference, also the NLO$'$ + gg result (green, dash-dotted) is shown in the ratio frame.
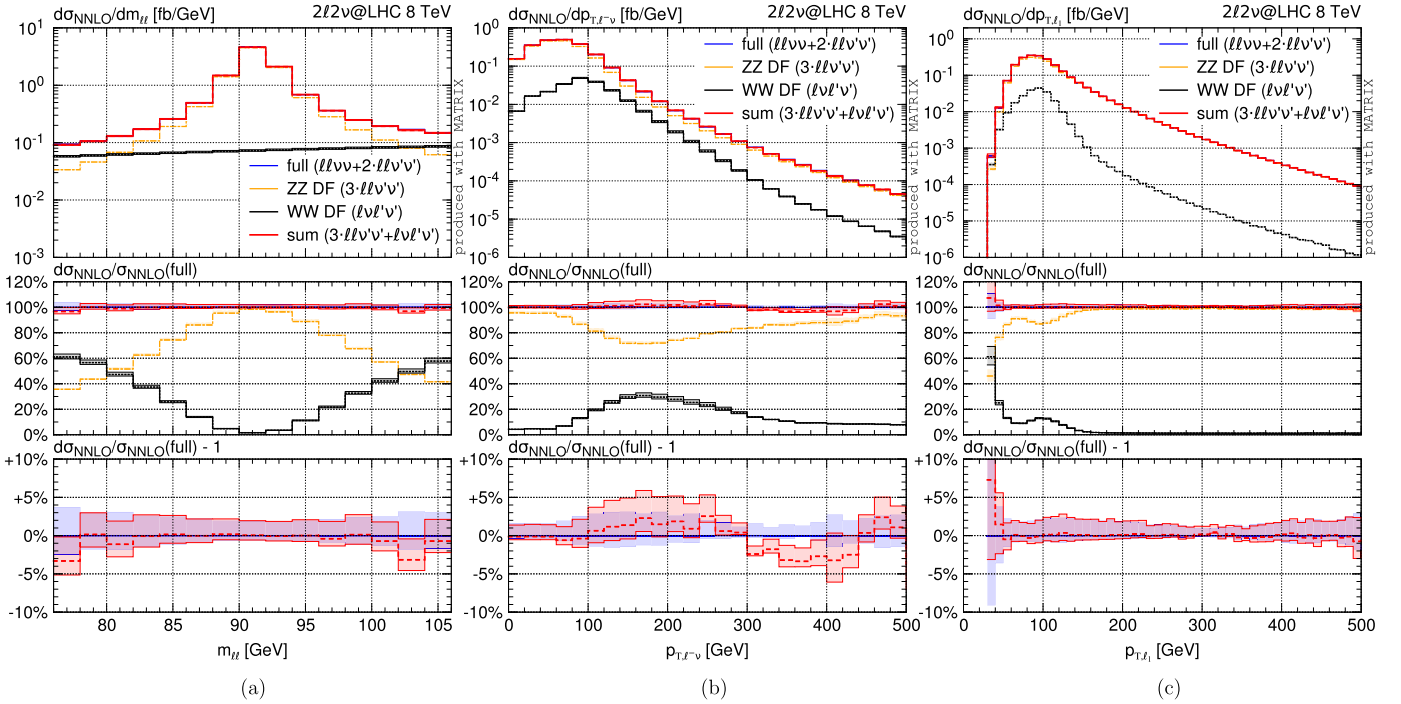

Fig. 6. Comparison of NNLO cross sections for the full process $\sigma(\ell\ell\,\nu_{e/\mu/\tau}\,\nu_{e/\mu/\tau})$ (blue, solid), the individual ZZ contributions $3 \cdot \sigma(\ell\ell\,\nu_{\ell'}\,\nu_{\ell'})$ with $\ell \neq \ell'$ (orange, dash-dotted), the individual W^+W^- contributions $\sigma(\ell\nu_\ell\,\ell'\nu_{\ell'})$ with $\ell \neq \ell'$ (black, dotted), and the approximation of the full result by the incoherent sum of ZZ and W^+W^- contributions $3 \cdot \sigma(\ell\ell\,\nu_{\ell'}\,\nu_{\ell'}) + \sigma(\ell\ell'\,\nu_\ell\,\nu_{\ell'})$ (red, dashed); for (a) $m_{\ell^+\ell^-}$, (b) $p_{T,\ell^-\nu}$, and (c) p_{T,ℓ_1}; the lower frames show the ratio to the full result.

$\sigma(\ell\ell\,\nu_\ell\nu_\ell) + 2 \cdot \sigma(\ell\ell\,\nu_{\ell'}\nu_{\ell'})$ for $\ell \in \{e, \mu\}$ and $\ell \neq \ell'$ with the same NNLO cross section, where the SF channel is approximated by the incoherent sum of the two DF processes, $\sigma(\ell\ell\,\nu_{e/\mu/\tau}\,\nu_{e/\mu/\tau}) \approx 3 \cdot \sigma(\ell\ell\,\nu_{\ell'}\,\nu_{\ell'}) + \sigma(\ell\nu_\ell\,\ell'\nu_{\ell'})$. The difference of the two is precisely the remaining interference contribution of ZZ with W^+W^- (and top-quark) topologies which we want to study. For completeness, also the individual DF ZZ and DF W^+W^- cross sections, $3 \cdot \sigma(\ell\ell\,\nu_{\ell'}\,\nu_{\ell'})$ and $\sigma(\ell\ell'\,\nu_\ell\,\nu_{\ell'})$, respectively, are shown, whose sum is the approximated cross section.

It is instructive to consider the invariant mass of the charged leptons, $m_{\ell^+\ell^-}$, in Fig. 6 (panel a), which nicely illustrates the nature of the different results: Only ZZ topologies feature a resonance at $m_{\ell^+\ell^-} = m_Z$, while the DF W^+W^- prediction is almost

flat in this range of $m_{\ell^+\ell^-}$. It is clear from the first ratio frame that almost the entire cross section around the peak stems from ZZ contributions. Only away from the peak W^+W^- production becomes larger than ZZ production. It is also clear that it is the $m_{\ell^+\ell^-}$ cut in the fiducial definition which significantly enhances ZZ contributions and suppresses the W^+W^- process. The relative difference between the approximated and the full result, which is enlarged in the second ratio frame, is very small, in particular in the peak region. This demonstrates that interference effects of ZZ with W^+W^- (and top-quark) topologies are negligible, and that an incoherent sum of the two DF channels is an excellent approximation of the SF process. This also implies that in our previous definition of the $\ell\ell + E_T^{\text{miss}}$ signature the remaining in-

terference effects after subtraction of W^+W^- and top-quark backgrounds are small. In fact, we hardly found any distribution with larger interference effects. The most pronounced example is the "pseudo"-observable in Fig. 6 (panel b) that shows the transverse-momentum spectrum of a W^- boson reconstructed as $\ell^- \nu_\ell$, and even in this case the differences do not exceed a few percent, although the shape is slightly deformed. With interference effects being generally small, it is interesting to analyse the different behaviour of ZZ and W^+W^- topologies. In the p_{T,ℓ_1} distribution in Fig. 6 (panel c), for example, the relative W^+W^- contribution increases around $p_{T,\ell_1} = 90$ GeV. This feature is already present at LO, and it is caused by purely kinematic effects that allow the two W bosons to become resonant simultaneously only in this part of phase space. The region below $p_{T,\ell_1} = 45$ GeV is populated only beyond LO.

We have presented NNLO QCD corrections to ZZ production for all leptonic processes. The $\ell\ell + E_T^{\text{miss}}$ signature has been studied for the first time at this level of accuracy, and we have introduced a procedure to compute results consistently in the five-flavour scheme without contributions from W^+W^- or top-quark backgrounds. We also computed state-of-the-art predictions for signatures involving four charged leptons. Our results are compared to ATLAS data at 8 TeV, and we find good agreement for both fiducial cross sections and distributions. NNLO QCD corrections are sizable, even in presence of a jet veto used in the $\ell\ell + E_T^{\text{miss}}$ measurement. By and large, they are of the order of 5%–20%, but can reach even 60% in certain phase-space regions. Most importantly, such effects do not only stem from the loop-induced gg contribution, but are also due to the newly computed genuine $\mathcal{O}(\alpha_S^2)$ corrections to the $q\bar{q}$ channel. Not least, we have shown that all remaining interference effects of ZZ topologies with W^+W^- and top-quark backgrounds in $2\ell2\nu$ production are negligible. The availability of fully differential NNLO predictions for all leptonic channels of ZZ production will play a crucial role in the rich physics programme that is based on precision studies of ZZ signatures at the LHC. Along with the paper we provide an updated version of Matrix, featuring all processes with the fiducial setup, cuts and distributions considered here.

Acknowledgements

References

[1] ATLAS, CMS, ATLAS-CONF-2016-036, CMS-PAS-SMP-15-001.
[2] G. Aad, et al., ATLAS, Phys. Rev. Lett. 108 (2012) 041804, arXiv:1110.5016 [hep-ex].
[3] S. Chatrchyan, et al., CMS, J. High Energy Phys. 01 (2013) 063, arXiv:1211.4890 [hep-ex].
[4] G. Aad, et al., ATLAS, J. High Energy Phys. 03 (2013) 128, arXiv:1211.6096 [hep-ex].
[5] S. Chatrchyan, et al., CMS, Phys. Lett. B 721 (2013) 190, arXiv:1301.4698 [hep-ex].
[6] V. Khachatryan, et al., CMS, Phys. Lett. B 740 (2015) 250, arXiv:1406.0113 [hep-ex].
[7] V. Khachatryan, et al., CMS, Eur. Phys. J. C 75 (2015) 511, arXiv:1503.05467 [hep-ex].
[8] G. Aad, et al., ATLAS, Phys. Lett. B 753 (2016) 552, arXiv:1509.07844 [hep-ex].
[9] M. Aaboud, et al., ATLAS, J. High Energy Phys. 01 (2017) 099, arXiv:1610.07585 [hep-ex].
[10] G. Aad, et al., ATLAS, Phys. Rev. Lett. 116 (2016) 101801, arXiv:1512.05314 [hep-ex].
[11] V. Khachatryan, et al., CMS, Phys. Lett. B 763 (2016) 280, arXiv:1607.08834 [hep-ex]; Erratum: Phys. Lett. B 772 (2017) 884.
[12] M. Aaboud, et al., ATLAS, Phys. Rev. D 97 (2018) 032005, arXiv:1709.07703 [hep-ex].
[13] A.M. Sirunyan, et al., CMS, Eur. Phys. J. C 78 (2018) 165, arXiv:1709.08601 [hep-ex].
[14] M. Aaboud, et al., ATLAS, Eur. Phys. J. C 78 (2018) 293, arXiv:1712.06386 [hep-ex].
[15] J. Ohnemus, J. Owens, Phys. Rev. D 43 (1991) 3626.
[16] B. Mele, P. Nason, G. Ridolfi, Nucl. Phys. B 357 (1991) 409.
[17] J. Ohnemus, Phys. Rev. D 50 (1994) 1931, arXiv:hep-ph/9403331.
[18] J.M. Campbell, R.K. Ellis, Phys. Rev. D 60 (1999) 113006, arXiv:hep-ph/9905386.
[19] L.J. Dixon, Z. Kunszt, A. Signer, Phys. Rev. D 60 (1999) 114037, arXiv:hep-ph/9907305.
[20] L.J. Dixon, Z. Kunszt, A. Signer, Nucl. Phys. B 531 (1998) 3, arXiv:hep-ph/9803250.
[21] E. Accomando, A. Denner, A. Kaiser, Nucl. Phys. B 706 (2005) 325, arXiv:hep-ph/0409247.
[22] A. Bierweiler, T. Kasprzik, J.H. Kühn, J. High Energy Phys. 1312 (2013) 071, arXiv:1305.5402 [hep-ph].
[23] J. Baglio, L.D. Ninh, M.M. Weber, Phys. Rev. D 88 (2013) 113005, arXiv:1307.4331 [hep-ph].
[24] B. Biedermann, A. Denner, S. Dittmaier, L. Hofer, B. Jäger, Phys. Rev. Lett. 116 (2016) 161803, arXiv:1601.07787 [hep-ph].
[25] B. Biedermann, A. Denner, S. Dittmaier, L. Hofer, B. Jäger, J. High Energy Phys. 01 (2017) 033, arXiv:1611.05338 [hep-ph].
[26] S. Kallweit, J.M. Lindert, S. Pozzorini, M. Schönherr, J. High Energy Phys. 11 (2017) 120, arXiv:1705.00598 [hep-ph].
[27] T. Binoth, T. Gleisberg, S. Karg, N. Kauer, G. Sanguinetti, Phys. Lett. B 683 (2010) 154, arXiv:0911.3181 [hep-ph].
[28] E.W.N. Glover, J.J. van der Bij, Nucl. Phys. B 321 (1989) 561.
[29] D.A. Dicus, C. Kao, W.W. Repko, Phys. Rev. D 36 (1987) 1570.
[30] T. Matsuura, J. van der Bij, Z. Phys. C 51 (1991) 259.
[31] C. Zecher, T. Matsuura, J. van der Bij, Z. Phys. C 64 (1994) 219, arXiv:hep-ph/9404295.
[32] T. Binoth, N. Kauer, P. Mertsch, Proc. DIS 2008 (2008) 142, arXiv:0807.0024 [hep-ph].
[33] J.M. Campbell, R.K. Ellis, C. Williams, J. High Energy Phys. 1107 (2011) 018, arXiv:1105.0020 [hep-ph].
[34] N. Kauer, J. High Energy Phys. 12 (2013) 082, arXiv:1310.7011 [hep-ph].
[35] F. Cascioli, S. Höche, F. Krauss, P. Maierhöfer, S. Pozzorini, F. Siegert, J. High Energy Phys. 1401 (2014) 046, arXiv:1309.0500 [hep-ph].
[36] J.M. Campbell, R.K. Ellis, C. Williams, J. High Energy Phys. 04 (2014) 060, arXiv:1311.3589 [hep-ph].
[37] J.M. Campbell, R.K. Ellis, C. Williams, PoS LL2014 (2014) 008, arXiv:1408.1723 [hep-ph].
[38] N. Kauer, C. O'Brien, E. Vryonidou, J. High Energy Phys. 10 (2015) 074, arXiv:1506.01694 [hep-ph].
[39] F. Caola, K. Melnikov, R. Röntsch, L. Tancredi, Phys. Rev. D 92 (2015) 094028, arXiv:1509.06734 [hep-ph].
[40] F. Caola, M. Dowling, K. Melnikov, R. Röntsch, L. Tancredi, J. High Energy Phys. 07 (2016) 087, arXiv:1605.04610 [hep-ph].
[41] S. Alioli, F. Caola, G. Luisoni, R. Röntsch, Phys. Rev. D 95 (2017) 034042, arXiv:1609.09719 [hep-ph].
[42] F. Caola, J.M. Henn, K. Melnikov, A.V. Smirnov, V.A. Smirnov, J. High Energy Phys. 1506 (2015) 129, arXiv:1503.08759 [hep-ph].
[43] A. von Manteuffel, L. Tancredi, J. High Energy Phys. 1506 (2015) 197, arXiv:1503.08835 [hep-ph].
[44] F. Cascioli, T. Gehrmann, M. Grazzini, S. Kallweit, P. Maierhöfer, A. von Manteuffel, S. Pozzorini, D. Rathlev, L. Tancredi, E. Weihs, Phys. Lett. B 735 (2014) 311, arXiv:1405.2219 [hep-ph].
[45] G. Heinrich, S. Jahn, S.P. Jones, M. Kerner, J. Pires, J. High Energy Phys. 03 (2018) 142, arXiv:1710.06294 [hep-ph].
[46] T. Gehrmann, A. von Manteuffel, L. Tancredi, E. Weihs, J. High Energy Phys. 1406 (2014) 032, arXiv:1404.4853 [hep-ph].
[47] F. Caola, J.M. Henn, K. Melnikov, A.V. Smirnov, V.A. Smirnov, J. High Energy Phys. 1411 (2014) 041, arXiv:1408.6409 [hep-ph].
[48] T. Gehrmann, A. von Manteuffel, L. Tancredi, J. High Energy Phys. 09 (2015) 128, arXiv:1503.04812 [hep-ph].
[49] M. Grazzini, S. Kallweit, D. Rathlev, Phys. Lett. B 750 (2015) 407, arXiv:1507.06257 [hep-ph].
[50] M. Grazzini, S. Kallweit, M. Wiesemann, arXiv:1711.06631 [hep-ph].
[51] A. Denner, S. Dittmaier, L. Hofer, PoS LL2014 (2014) 071, arXiv:1407.0087 [hep-ph].
[52] A. Denner, S. Dittmaier, L. Hofer, Comput. Phys. Commun. 212 (2017) 220, arXiv:1604.06792 [hep-ph].
[53] G. Ossola, C.G. Papadopoulos, R. Pittau, J. High Energy Phys. 0803 (2008) 042, arXiv:0711.3596 [hep-ph].
[54] A. van Hameren, Comput. Phys. Commun. 182 (2011) 2427, arXiv:1007.4716 [hep-ph].
[55] F. Cascioli, P. Maierhöfer, S. Pozzorini, Phys. Rev. Lett. 108 (2012) 111601, arXiv:1111.5206 [hep-ph].

[56] F. Buccioni, S. Pozzorini, M. Zoller, Eur. Phys. J. C 78 (2018) 70, arXiv:1710.11452 [hep-ph].

[57] S. Catani, M. Grazzini, Phys. Rev. Lett. 98 (2007) 222002, arXiv:hep-ph/0703012.

[58] S. Kallweit, J.M. Lindert, P. Maierhöfer, S. Pozzorini, M. Schönherr, J. High Energy Phys. 04 (2015) 012, arXiv:1412.5157 [hep-ph].

[59] S. Kallweit, J.M. Lindert, P. Maierhöfer, S. Pozzorini, M. Schönherr, J. High Energy Phys. 04 (2016) 021, arXiv:1511.08692 [hep-ph].

[60] S. Kallweit, Munich is the abbreviation of "MUlti-chaNnel Integrator at Swiss (CH) precision"—an automated parton level NLO generator, in preparation..

[61] S. Catani, M. Seymour, Phys. Lett. B 378 (1996) 287, arXiv:hep-ph/9602277.

[62] S. Catani, M. Seymour, Nucl. Phys. B 485 (1997) 291, arXiv:hep-ph/9605323.

[63] M. Grazzini, S. Kallweit, D. Rathlev, A. Torre, Phys. Lett. B 731 (2014) 204, arXiv:1309.7000 [hep-ph].

[64] M. Grazzini, S. Kallweit, D. Rathlev, J. High Energy Phys. 07 (2015) 085, arXiv:1504.01330 [hep-ph].

[65] T. Gehrmann, M. Grazzini, S. Kallweit, P. Maierhöfer, A. von Manteuffel, S. Pozzorini, D. Rathlev, L. Tancredi, Phys. Rev. Lett. 113 (2014) 212001, arXiv:1408.5243 [hep-ph].

[66] M. Grazzini, S. Kallweit, S. Pozzorini, D. Rathlev, M. Wiesemann, J. High Energy Phys. 08 (2016) 140, arXiv:1605.02716 [hep-ph].

[67] M. Grazzini, S. Kallweit, D. Rathlev, M. Wiesemann, Phys. Lett. B 761 (2016) 179, arXiv:1604.08576 [hep-ph].

[68] M. Grazzini, S. Kallweit, D. Rathlev, M. Wiesemann, J. High Energy Phys. 05 (2017) 139, arXiv:1703.09065 [hep-ph].

[69] D. de Florian, M. Grazzini, C. Hanga, S. Kallweit, J.M. Lindert, P. Maierhöfer, J. Mazzitelli, D. Rathlev, J. High Energy Phys. 09 (2016) 151, arXiv:1606.09519 [hep-ph].

[70] M. Grazzini, G. Heinrich, S. Jones, S. Kallweit, M. Kerner, J.M. Lindert, J. Mazzitelli, J. High Energy Phys. 05 (2018) 059, arXiv:1803.02463 [hep-ph].

[71] M. Grazzini, S. Kallweit, D. Rathlev, M. Wiesemann, J. High Energy Phys. 08 (2015) 154, arXiv:1507.02565 [hep-ph].

[72] E. Re, M. Wiesemann, G. Zanderighi, arXiv:1805.09857 [hep-ph].

[73] A. Denner, S. Dittmaier, M. Roth, L.H. Wieders, Nucl. Phys. B 724 (2005) 247, arXiv:hep-ph/0505042; Erratum: Nucl. Phys. B 854 (2012) 504.

[74] C. Patrignani, et al., Particle Data Group, Chin. Phys. C 40 (2016) 100001.

[75] R.D. Ball, et al., NNPDF, J. High Energy Phys. 1504 (2015) 040, arXiv:1410.8849 [hep-ph].

[76] P. Nason, J. High Energy Phys. 11 (2004) 040, arXiv:hep-ph/0409146.

[77] S. Frixione, P. Nason, C. Oleari, J. High Energy Phys. 11 (2007) 070, arXiv:0709.2092 [hep-ph].

[78] S. Alioli, P. Nason, C. Oleari, E. Re, J. High Energy Phys. 06 (2010) 043, arXiv:1002.2581 [hep-ph].

[79] T. Melia, P. Nason, R. Röntsch, G. Zanderighi, J. High Energy Phys. 11 (2011) 078, arXiv:1107.5051 [hep-ph].

[80] P.F. Monni, G. Zanderighi, J. High Energy Phys. 1505 (2015) 013, arXiv:1410.4745 [hep-ph].